

Anti-correlation between the mass of a supermassive black hole and the mass accretion rate in type I ultraluminous infrared galaxies and nearby QSOs

Nozomu Kawakatu¹

National Astronomical Observatory of Japan, 2-21-1 Osawa, Mitaka, Tokyo 181-8588, Japan

Masatoshi Imanishi

National Astronomical Observatory of Japan, 2-21-1, Osawa, Mitaka, Tokyo 181-8588, Japan

Tohru Nagao

National Astronomical Observatory of Japan, 2-21-1 Osawa, Mitaka, Tokyo 181-8588, Japan

ABSTRACT

We discovered a significant anti-correlation between the mass of a supermassive black hole (SMBH), M_{BH} , and the luminosity ratio of infrared to active galactic nuclei (AGN) Eddington luminosity, $L_{\text{IR}}/L_{\text{Edd}}$, over four orders of magnitude for ultraluminous infrared galaxies with type I Seyfert nuclei (type I ULIRGs) and nearby QSOs. This anti-correlation (M_{BH} vs. $L_{\text{IR}}/L_{\text{Edd}}$) can be interpreted as the anti-correlation between the mass of a SMBH and the rate of mass accretion onto a SMBH normalized by the AGN Eddington rate, $\dot{M}_{\text{BH}}/\dot{M}_{\text{Edd}}$. In other words, the mass accretion rate \dot{M}_{BH} is not proportional to that of the central BH mass. Thus, this anti-correlation indicates that BH growth is determined by the external mass supply process, and not the AGN Eddington-limited mechanism. Moreover, we found an interesting tendency for type I ULIRGs to favor a super-Eddington accretion flow, whereas QSOs tended to show a sub-Eddington flow. On the basis of our findings, we suggest that a central SMBH grows by changing its mass accretion rate from super-Eddington to sub-Eddington. According to a coevolution scenario of ULIRGs and QSOs based on the radiation drag process, it has been predicted that a self-gravitating massive torus, whose mass is larger

¹kawakatu@th.nao.ac.jp

than a central BH, exists in the early phase of BH growth (type I ULIRG phase) but not in the final phase of BH growth (QSO phase). At the same time, if one considers the mass accretion rate onto a central SMBH via a turbulent viscosity, the anti-correlation (M_{BH} vs. $L_{\text{IR}}/L_{\text{Edd}}$) is well explained by the positive correlation between the mass accretion rate \dot{M}_{BH} and the mass ratio of a massive torus to a SMBH.

Subject headings: galaxies:active — galaxies:bulges — galaxies:formation — galaxies:starburst — quasars:general — black hole — infrared:galaxies

1. Introduction

Ultraluminous infrared galaxies (ULIRGs) radiate QSO-like (= high luminosity AGN) luminosities ($> 10^{12}L_{\odot}$) as infrared dust emission, and their space densities are similar to those of QSOs (e.g., Sanders & Mirabel 1996). The AGN phenomenon appears in the final merging stage, and the percentage of AGNs increases with infrared luminosity reaching 30 – 50% for $L_{\text{IR}} > 10^{12}L_{\odot}$ (Veilleux et al. 1999). The near-infrared light distributions in many ULIRGs appear to fit a de Vaucouleur’s profile, which is representative of elliptical galaxies (Scoville et al. 2000; Veilleux et al. 2002). Plenty of molecular gas exists in their central kpc regions (e.g., Downes & Solomon 1998; Bryant & Scoville 1999; Gao & Solomon 2004; Imanishi et al. 2006a), with gas mass densities comparable to stellar densities in elliptical galaxies. As for QSOs, their hosts are mostly luminous and well evolved early-type galaxies (e.g., McLeod & Rieke 1995; Bahcall et al. 1997; McLure et al. 2000; Dunlop et al. 2003). Kormendy & Sanders (1992) proposed that ULIRGs evolve into ellipticals through merger-induced dissipative collapse. Under this scenario, these mergers first go through a luminous starburst phase, then enter a dust-enshrouded AGN phase, and finally evolve into optically bright QSOs after they shed the dusty gas (Sanders et al. 1988). Until recently, it was believed that supermassive black holes (SMBHs) were a basic component of galaxies, and that the mass of a SMBH was tightly correlated to the mass, velocity dispersion, and luminosity of bulges (e.g., Kormendy & Richstone 1995; Laor 1998; Magorian et al. 1998; Richstone et al. 1998; Ferrarese & Merritt 2000; McLure & Dunlop 2001, 2002; Tremaine et al. 2002; Marconi & Hunt 2003; Kawakatu & Umemura 2004). Combined with the ULIRG-QSO connection, these findings imply that SMBH growth and starburst (progenitors of ellipticals) are physically connected. However, the evolutionary track between ULIRGs and QSOs has been an issue of long standing.

Canalizo & Stockton (2001) proposed that ULIRGs with type I Seyfert nuclei (hereafter type I ULIRGs) are the transitional stage between ULIRGs and QSOs because their host

galaxies are undergoing tidal interactions. In addition, type I ULIRGs have a tendency to be advanced mergers with single nuclei (Veilleux et al. 2002). Thus, type I ULIRGs have the attraction of the Rosetta Stone as far as revealing the physical relationship between ULIRGs and QSOs. Most of them show a full-width at half-maximum (FWHM) of the broad $H\beta$ line of less than 2000 km s^{-1} (Moran et al. 1996; Zheng et al. 2002; hereafter Z02), and thus AGNs in type I ULIRGs would actually be narrow-line Seyfert 1 galaxies (NLS1s). Recent *Chandra* observations (Teng et al. 2005) discovered that two type I ULIRGs (IRAS [*Infrared Astronomical Satellite*] F01572+0009 and IRAS Z11598–0112) show a soft X-ray excess and a steep photon index ($\Gamma_{2-10 \text{ keV}} > 2$), which are characteristic properties of NLS1s. All of these results suggest that type I ULIRGs have a tendency to harbor NLS1-like nuclei. Noting the similarities between NLS1s and type I ULIRGs, one possible interpretation is that type I ULIRGs have smaller central BHs than QSOs and that their BHs are rapidly growing (e.g., Pounds et al. 1995; Boller et al. 1996; Mineshige et al. 2000; Kawaguchi 2003; Collin & Kawaguchi 2004; Shemmer et al. 2006). Moreover, Kawakatu et al. (2006; hereafter K06) found that type I ULIRGs have a BH mass one order of magnitude smaller despite having the comparable R -band bulge luminosity (M_R) relative to QSOs and elliptical galaxies. They also showed that most type I ULIRGs are located near a proto-QSO phase, which is the early phase of BH growth predicted by a coevolution scenario of galactic bulges and SMBHs (Kawakatu et al. 2003; hereafter KUM03). These findings support a scenario in which type I ULIRGs are in the transition stage from ULIRGs to QSOs. However, little is understood about how SMBHs grow in the evolutionary sequence from ULIRGs to QSOs. To address this issue, we elucidated the relationship between the mass of a SMBH and the mass accretion rate normalized by the AGN Eddington rate in type I ULIRGs and QSOs. To this end, we derived the mass accretion rate normalized by the AGN Eddington rate from the ratio of AGN bolometric luminosity to AGN Eddington luminosity. Note that the infrared luminosity at $8\text{--}1000 \mu\text{m}$ (not far-infrared luminosity) is a good indicator of AGN activities for type I AGNs (type I ULIRGs and QSOs). We discuss the validity of this treatment later.

This article is arranged as follows. In §2, we describe how type I ULIRGs and QSOs were selected to achieve our aim. In §3, we discuss how we evaluated SMBH mass and infrared luminosity for type I ULIRGs and QSOs. Moreover, we comment on the origin of infrared luminosity in type I ULIRGs and QSOs. In §4, we show the anti-correlation between the ratio of infrared to AGN Eddington luminosity and BH mass. Then, we discuss what scientists can learn from this anti-correlation. Finally, we devote §5 to discussions and conclusions. Throughout this article, we adopt the Hubble parameter $H_0 = 75 \text{ km s}^{-1} \text{ Mpc}^{-1}$ and the deceleration parameter $q_0 = 0.5$; we have converted results from published articles to this cosmology to facilitate comparisons.

2. Sample Selection

To accomplish our aim, we used a type I ULIRG sample and an optically selected QSO sample, for which the data of FWHM (broad $H\beta$ line), the optical luminosity at 5100\AA in the rest frame, and the infrared luminosity were available. The details of these samples are as follows:

(1) The type I ULIRG sample was from Z02. This sample was compiled from ULIRGs in the QDOT (Queen Mary and Westfield College, Durham, Oxford, and Toronto) redshift survey (Lawrence et al. 1999), the 1Jy ULIRG survey (Kim & Sanders 1998), and an IR QSO sample selected from the cross-correlation of the IRAS Point-Source Catalog with the ROSAT (*Röntgensatellit*) All-Sky Survey Catalog (Boller et al. 1992). All type I ULIRGs selected by Z02 were ULIRGs with mid- to far-infrared properties from IRAS observations. From these samples, we selected all 23 objects for which Z02 provided data on both the width of the broad $H\beta$ line and the luminosity at 5100\AA in the rest frame. Except for IRAS F16136+6550, infrared luminosities $L_{\text{IR}} = L_{8-1000\ \mu\text{m}}$ were greater than $10^{12}L_{\odot}$. All of them were at $\delta > -30$ degree, and they constituted $\sim 30\%$ of all type I ULIRGs identified in the largest IRAS redshift survey, thus providing a representative sample of all type I ULIRGs. In addition, all type I ULIRGs were final merging (single-nucleus) objects (Veilleux et al. 2002), and the average redshift was $z \approx 0.2$.

(2) The optically selected QSO sample comprised 47 Palomar Green quasars (PG QSOs) from Boroson & Green (1992; hereafter BG92). We excluded PG 0157+001 (Mrk 1014) and PG 1226+023 (3C 273) from the PG QSO sample because they are categorized as type I ULIRGs. We added 11 PG QSOs observed by McLure & Dunlope (2001; hereafter MD01). Our sample criteria were known data on the width of broad $H\beta$ line, luminosity at 5100\AA in the rest frame, and infrared luminosity. The average redshift of the selected QSO sample was around 0.2, and thus the redshift distribution of the PG QSOs was similar to that of the type I ULIRGs. Infrared flux for all 58 PG QSOs was taken from the IRAS Faint Source Catalog (Sanders et al. 1989), IRAS Point Source Catalog, or ISO Catalog (Haas et al. 2003).

We summarize basic physical parameters of the type I ULIRGs and PG QSOs in Tables 1-3.

3. Estimation of Physical Parameters

3.1. Black Hole Masses

To evaluate central SMBH mass, we assumed that the motion of ionized gas clouds moving around the BH is dominated by gravitational force and that the clouds within the broad-line region (BLR) are virialized (e.g., Peterson & Wandel 1999, 2000). Thus, central SMBH mass can be expressed as $M_{\text{BH}} \approx R_{\text{BLR}}v^2/G$, where v is the velocity dispersion of matter at the radius of the BLR R_{BLR} , which is the distance of the emission-line clouds responding to the central continuum variation as determined from reverberation mappings. Then, central mass can be estimated as

$$M_{\text{BH}} = 1.5 \times 10^5 \left(\frac{R_{\text{BLR}}}{\text{lt} - \text{days}} \right) \left(\frac{v_{\text{FWHM}}}{10^3 \text{km s}^{-1}} \right)^2 M_{\odot}. \quad (1)$$

The velocity dispersion v can be estimated from the FWHM of $\text{H}\beta$ broad-line emission $v = fv_{\text{FWHM}}$ by assuming the BLR gas to be in isotropic motion ($f = \sqrt{3}/2$). Kaspi et al. (2000) found an empirical relationship between the size of the BLR, R_{BLR} , and optical continuum luminosity, $\lambda L_{\lambda}(5100\text{\AA})_{\text{rest}}$, on the basis of 17 Seyfert galaxies and 17 optically selected PG QSOs.

$$R_{\text{BLR}} = 32.9_{-1.9}^{+2.0} \left[\frac{\lambda L_{\lambda}(5100\text{\AA})_{\text{rest}}}{10^{44} \text{erg s}^{-1}} \right]^{0.70 \pm 0.033} \text{light} - \text{days}. \quad (2)$$

By combining equations (1) and (2), we obtain the following formula:

$$M_{\text{BH}} = 4.9_{-0.3}^{+0.4} \times 10^6 \left[\frac{\lambda L_{\lambda}(5100\text{\AA})_{\text{rest}}}{10^{44} \text{erg s}^{-1}} \right]^{0.70 \pm 0.033} \left(\frac{v_{\text{FWHM}}}{10^3 \text{km s}^{-1}} \right)^2 M_{\odot}. \quad (3)$$

Note that equation (2) holds not only for broad-line type I AGNs but also for NLS1s (Peterson et al. 2000). To evaluate the optical luminosity at 5100\AA in the rest frame, $L_{\lambda}(5100\text{\AA})_{\text{rest}}$, we used the formula $L_{\lambda}(5100\text{\AA})_{\text{rest}} = 4\pi d_L^2(1+z)F_{\lambda}(5100(1+z)\text{\AA})_{\text{obs}}$, where d_L is the luminosity distance. For 23 type I ULIRGs, the FWHM ($\text{H}\beta$) and the observed flux at 5100\AA , $F_{\lambda}(5100(1+z)\text{\AA})_{\text{obs}}$, were given by Z02 and measured directly from their spectra. For 48 PG QSOs in our sample, the FWHM of $\text{H}\beta$ measurements were from BG92. It is reasonable to expect that the 5100\AA continuum flux measured using a $15''$ aperture (Neugebauer et al. 1987) is dominated by a central AGN emission in the QSO sample (= high luminosity AGN). The flux densities at 5100\AA were approximated by linear interpolation. For most PG QSOs, this was performed over neighboring frequency ranges in relatively tight SEDs, and thus this

treatment is reliable. For a few objects, $L_\lambda(5100\text{\AA})_{\text{rest}}$ was computed by 4400\AA flux density (Kellerman et al. 1989). Assuming a power-law continuum $F_\nu \propto \nu^\alpha$ with a median optical slope of $\alpha = \alpha_{\text{opt}} = -0.2$ (Neugebauer et al. 1987), we extrapolated to 5100\AA . For the other 11 PG QSOs, we adopted data from the MD01 database.

Finally, the uncertainties of SMBH mass were estimated by error propagating using the optical luminosity at 5100\AA and the FWHM of the $H\beta$ measurements. The mean error of SMBH mass was a factor of 1.3. In general, SMBH mass computed in this way [eq. (3)] is systematically accurate to within a factor of 3 (e.g., Wang & Lu 2001; Marziani et al. 2003; Schemmer et al. 2004).

3.2. Infrared Luminosities

We evaluated infrared luminosities using the following formula (Sanders & Mirabel 1996) based on the flux densities from the IRAS Faint Source Catalog (Sanders et al. 1989), IRAS Point Source Catalog, and ISO Catalog (Haas et al. 2003):

$$L_{\text{IR}}[8 - 1000\mu\text{m}] = 4\pi d_L^2 F_{\text{IR}}, \quad (4)$$

where F_{IR} is defined as

$$F_{\text{IR}} = 1.8 \times 10^{-14} (13.48f_{12} + 5.16f_{25} + 2.58f_{60} + f_{100}) \text{ W m}^{-2} \quad (5)$$

with f_{12} , f_{25} , f_{60} and f_{100} being the IRAS or ISO flux densities at 12, 25, 60, and 100 μm in units of Jy.

For sources with upper limits in some bands, we calculated upper and lower values of infrared luminosities in the following ways. The upper value was estimated by employing the upper limit in some bands as the actual value. The lower value was determined by adopting zero values. If the difference between them was very small (less than 0.2 dex, which would not affect our main results), we applied the upper value in this article. If not, we show both the upper and lower values. As for objects with upper limits in all four bands, upper limits of infrared luminosities only are shown in Table 1.

3.3. Origin of infrared luminosities in type I ULIRGs and QSOs

In the next section (§4), we present the M_{BH} vs. $L_{\text{IR}}/L_{\text{Edd}}$ relationship and comment on its physical meaning. Before we do, however, we discuss the origin of L_{IR} in type I ULIRGs

and QSOs.

Concerning the origin of L_{IR} of QSOs: The warmer dust emission ($T \sim 200$ K) that dominates the mid-infrared ($12 \mu\text{m}$ and $25 \mu\text{m}$) SEDs of QSOs is accepted as being predominantly AGN heated (e.g., Rowan-Robinson 1995; Haas et al. 2000, 2003). However, the origin of the cooler dust emission ($T \sim 50$ K) that dominates the far-infrared ($60 \mu\text{m}$ and $100 \mu\text{m}$) SEDs is still under debate (e.g., Sanders et al. 1989; Rowan-Robinson 1995; Haas et al. 2003; Ho 2005). Recently, Schweitzer et al. (2006) found that the ratio of polycyclic aromatic hydrocarbon (PAH) luminosity ¹ to far-infrared luminosity ($L_{\text{FIR}} = \nu L_{\nu}(60\mu\text{m})$) is 10 – 30% in bona fide starburst galaxies. This indicates that a starburst contributes 10 – 30% of L_{FIR} . Because $L_{\text{IR}} > L_{\text{FIR}}$ (by definition) and L_{IR} is significantly larger L_{FIR} for QSOs (e.g., Haas et al. 2003), its contribution is less than 10 – 30% for L_{IR} . Therefore, the contribution of AGNs is more than 70 – 90% for L_{IR} ; in other words, L_{IR} in QSOs is dominated by AGN power.

As for type I ULIRGs, Imanishi et al. (2006b; hereafter I06b) showed that 40%(9/23) of type I ULIRGs have substantially smaller ratios of $3.3 \mu\text{m}$ PAH to infrared than starburst-dominated galaxies, whose luminosity ratios $L_{3.3\mu\text{mPAH}}/L_{\text{IR(SB)}}$ are $\sim 10^{-3}$ (e.g., Mouri et al. 1990; Imanishi 2002). The scatter of PAH to the infrared luminosity ratio is a factor of 2 – 3 (Fischer et al. 2000). Note that dust extinction in the L -band ($2.8 - 4.1 \mu\text{m}$) is less than 1 mag because $A_L \sim 0.06A_V$, where A_V is the optical extinction (Rieke & Lebofsky 1985; Lutz et al. 1996). Thus, the small $L_{3.3\mu\text{m,PAH}}/L_{\text{IR(SB)}}$ suggests that the moderately obscured ($A_V < 15$ mag) nuclear starbursts ($< \text{kpc}$) can contribute only a small fraction ($< 30\%$) of the infrared luminosity (see Table 1). In addition, most type I ULIRGs show warm far-infrared colors ($f_{25}/f_{60} > 0.2$) ², where f_{25}/f_{60} is the IRAS or ISO $25 \mu\text{m}$ -to- $60 \mu\text{m}$ flux ratio. Thus, the contributions of the host starburst and the heavily obscured nuclear starburst ($A_V \gg 15$ mag) should be small. Moreover, the hard X-ray emission of two type I ULIRGs (IRAS F01572+0009 and IRAS Z11598–0112) with detected PAH emission is dominated by an AGN because their hard X-ray (2–10 keV)-to-AGN-bolometric-luminosity ratios are substantially larger than those in typical starburst galaxies (Teng et al. 2005). Therefore, these results indicate that the infrared luminosity of type I ULIRGs is powered by AGN activity.

Finally, we question whether L_{IR} is the best tracer of AGN activity in type I ULIRGs

¹PAH emission is a good indicator of starburst activity because emissions from PAH molecules are excited by far-UV photons in normal starburst galaxies, while PAH molecules can be destroyed by X-rays from AGN (Voit 1992).

²Warm infrared colors often appear in normal AGNs (e.g., de Grijp et al. 1987).

and QSOs. Hao et al. (2005) claimed that for most type I ULIRGs, starbursts play a major role in the far-infrared band, whereas AGNs contribute in the mid-infrared band. Thus, one may think that mid-infrared luminosity ($L_{\text{MIR}} = \nu L_{\nu}(12\mu\text{m})$ or $\nu L_{\nu}(25\mu\text{m})$) is a better tracer of AGN activities than L_{IR} . As shown in Fig. 1, the anti-correlation between M_{BH} and L_i/L_{Edd} can be seen in all four panels (Fig. 1a-d), where L_i is the monochromatic luminosity with $i = 12\mu\text{m}, 25\mu\text{m}, 60\mu\text{m}$ and $100\mu\text{m}$, although the slopes of these anti-correlations are slightly different. This suggests that the M_{BH} vs. $L_{\text{IR}}/L_{\text{Edd}}$ relationship (Fig. 2; see discussion in §4.) has the same physical meaning as the M_{BH} vs. $L_{\text{MIR}}/L_{\text{Edd}}$ relationship. Thus, the results we present in §4 do not change whether we employ L_{IR} or L_{MIR} . Next we note two advantages of using L_{IR} instead of L_{MIR} . One is that we can estimate both the upper and lower values of L_{IR} , even with non-detection at mid-infrared bands, as most objects are detected at far-infrared bands. Thus, if we were to employ L_{IR} , it would be possible to use a much larger sample (especially for type I ULIRGs; see Table 1) than for L_{MIR} , which is essential in statistical discussions. The other is that L_{IR} is closer than L_{MIR} to bolometric luminosity, which is important when discussing mass accretion rate onto a central BH. Taking account of the origin of L_{IR} as AGNs both in type I ULIRGs and QSOs and the advantages of using L_{IR} , L_{IR} is the better choice for examining the relationship between mass accretion rate and central BH mass for type I ULIRGs and QSOs.

4. Results

We plot the ratio of infrared to AGN Eddington luminosity, $L_{\text{IR}}/L_{\text{Edd}}$, vs. SMBH mass, M_{BH} , for 23 type I ULIRGs and 58 PG QSOs in Fig. 2. Filled squares denote type I ULIRGs, open squares show type I ULIRGs in which PAH emissions were detected, open circles and down arrows show broad-line QSOs (BLQSOs) whose FWHM of the broad $\text{H}\beta$ line is larger than 2000 km/s, and filled circles represent narrow-line QSOs (NLQSOs) whose FWHM of the broad $\text{H}\beta$ line is less than 2,000 km/s.

Figure 2 shows that $L_{\text{IR}}/L_{\text{Edd}}$ was well anti-correlated with M_{BH} over four orders of magnitude (Spearman’s correlation of rank coefficient $r_s = -0.791$). The thick solid line is the best-fitting relationship for all samples (type I ULIRGs and PG QSOs) except for the upper limit data, $\log(L_{\text{IR}}/L_{\text{Edd}}) = -0.961(\pm 0.081) \log M_{\text{BH}} + 7.06(\pm 0.65)$ with $\chi^2 = 0.319$. This line corresponds to the $L_{\text{IR}} \approx 10^{12} L_{\odot}$. The dashed line represents the best-fitting relationship for BLQSOs only except for the upper limit data, $\log(L_{\text{IR}}/L_{\text{Edd}}) = -0.369(\pm 0.108) \log M_{\text{BH}} + 1.89(\pm 0.028)$ ($\chi^2 = 0.149$). We found that the slope of the BLQSO sample was slightly shallower than those of the other targets. Next we discuss the physical meaning of the anti-correlation (M_{BH} vs. $L_{\text{IR}}/L_{\text{Edd}}$).

4.1. Mass accretion rate onto a SMBH in type I ULIRGs and QSOs

As shown in Fig. 2, most type I ULIRGs (19/23) had a ratio of infrared to AGN Eddington luminosity of $L_{\text{IR}}/L_{\text{Edd}} > 1$. The average value of $\log(L_{\text{IR}}/L_{\text{Edd}})$ was 0.525 (see Table 4). This indicates that the AGN bolometric luminosity (L_{bol}) of most type I ULIRGs is beyond that of an AGN Eddington luminosity because $L_{\text{IR}}/L_{\text{Edd}} = (L_{\text{IR}}/L_{\text{bol}}) \times (L_{\text{bol}}/L_{\text{Edd}})$ and $L_{\text{IR}}/L_{\text{bol}} < 1$ (by definition). Theoretically, BH accretion luminosity can achieve up to $\approx 10L_{\text{Edd}}$ (e.g., Ohsuga et al. 2005) in optically thick accretion disks called *slim disks* associated with super-Eddington accretion flow (e.g., Abramowicz et al. 1988; Wang et al. 1999; Mineshige et al. 2000; Kawaguchi 2003). Thus, we can conclude that super-Eddington accretion flow is a common feature of type I ULIRGs. To confirm this postulate, we evaluated the AGN bolometric luminosity from the hard X-ray luminosity for two detected type I ULIRGs, assuming a bolometric correction factor of $f_{2-10\text{keV}} = 30 - 85$ for bright AGNs (Marconi et al. 2004; Barger et al. 2005). Indeed, two type I ULIRGs (IRAS F01572+0009 and IRAS Z11598–0112) showed higher ratios of AGN bolometric luminosities than BLQSOs to AGN Eddington luminosities (e.g., McLeod et al. 1999), $-0.44 < \log(L_{\text{bol}}/L_{\text{Edd}}) < 0.01$ for F01572+009 and $0.18 < \log(L_{\text{bol}}/L_{\text{Edd}}) < 0.63$ for Z11598–0112 (see Table 5 in Teng et al. 2005). This supports the idea that type I ULIRGs favor higher mass accretion rates (\dot{M}_{BH}) than normal BLQSOs, although the sample was very limited. Note that $\log(L_{\text{bol}}/L_{\text{Edd}})$ derived from the X-ray luminosity is less than $\log(L_{\text{IR}}/L_{\text{Edd}})$, which may imply that the bolometric correction factor $f_{2-10\text{keV}}$ of type I ULIRGs is larger than that of BLQSOs. Examining the physical reasons for this in the future may prove to be worthwhile.

In contrast, the infrared luminosity was less than the AGN Eddington luminosity for $\approx 96\%$ of QSOs, with the average $\log(L_{\text{IR}}/L_{\text{Edd}}) = -1.06$ (Table 4). This coincides with previous findings that the mass accretion rate of normal QSOs is of the sub-Eddington type (e.g., McLeod et al. 1999). Interestingly, NLQSOs have a tendency to be higher $L_{\text{IR}}/L_{\text{Edd}}$ than BLQSOs, as shown in Fig. 2. Three NLQSOs (PG 0050+124, PG 1244+026, and PG 1402+261) with $L_{\text{IR}}/L_{\text{Edd}} \approx 1$ showed steep hard X-ray power-law photon index ($\Gamma_{2-10\text{keV}}$), which is characteristic of AGNs with super-critical accretion, like NLS1s. However, the $\Gamma_{2-10\text{keV}}$ of two NLQSOs with $L_{\text{IR}}/L_{\text{Edd}} < 1$ (PG 1211+143 and PG 1440+356) was less than 2 (Piconcelli et al. 2005). These findings confirm that $L_{\text{IR}}/L_{\text{Edd}}$ is a good indicator of the mass accretion rate onto a central BH for high-luminosity type I AGNs (type I ULIRGs and QSOs).

Veilleux et al. (2006) claimed that five type I ULIRGs (IRAS F07598+6508, IRAS F12540+5708, IRAS F13218+0552, IRAS F15462–0450, and IRAS F21219–1757) do not require super-Eddington accretion rates (see also Genzel et al. 2001; Tacconi et al. 2002), assuming an *H*-band early-type host magnitude-BH mass relation for well evolved early

type galaxies as described in Marconi & Hunt (2003). However, K06 showed that most type I ULIRGs are not satisfied with the local SMBH-bulge relationship, and thus their BH mass would be overestimated compared to values obtained by using our method [eq. (3)]. We emphasize that our conclusion (i.e., that type I ULIRGs tend to show a super-Eddington accretion rate) is based on the virial theorem without adopting the local SMBH-bulge relationship.

4.2. Origin of anti-correlation between M_{BH} and $L_{\text{IR}}/L_{\text{Edd}}$

In this section, we consider the origin of the anti-correlation between M_{BH} and $L_{\text{IR}}/L_{\text{Edd}}$ (Fig. 2). Two possible interpretations exist:

1. The ratio of infrared to AGN bolometric luminosity ($L_{\text{IR}}/L_{\text{bol}}$) is anti-proportional to the mass of a SMBH (M_{BH}), where $L_{\text{IR}}/L_{\text{bol}}$ reflects the geometry of the obscuring torus.
2. The ratio of the AGN bolometric to the AGN Eddington luminosity ($L_{\text{bol}}/L_{\text{Edd}}$) is anti-correlated to M_{BH} , where $L_{\text{bol}}/L_{\text{Edd}}$ is a tracer of the mass accretion rate normalized by the AGN Eddington mass accretion rate.

If case (1) is a main origin of the anti-correlation, the covering factor of the obscuring torus must decrease with the mass of a SMBH. The clouds photoionized by AGNs' hard radiation form the narrow-line region (NLR) at $\sim 10 - 1000$ pc distances from AGNs because AGNs in type I ULIRGs are obscured by dust in a torus-like geometry. Thus, the strong high-excitation forbidden line emissions from NLRs (e.g., [OIII] λ 5007) are detectable for type I ULIRGs and thus evaluate the degree of NLR development, which is reflected by the equivalent width of [OIII] λ 5007 at the rest frame $\text{EW}([\text{OIII}]\lambda 5007)$. The rest frame $\text{EW}([\text{OIII}]\lambda 5007)$ of type I ULIRGs and PG QSOs can be taken from Z02 and BG92, respectively. Note that we did not use the upper values of the rest frame $\text{EW}([\text{OIII}]\lambda 5007)$ for four type I ULIRGs (see Table 2). If the anti-correlation shows the difference of the obscuring geometry between type I ULIRGs and QSOs, the rest frame $\text{EW}([\text{OIII}]\lambda 5007)$ of type I ULIRGs should be smaller than that of PG QSOs because the rest frame $\text{EW}([\text{OIII}]\lambda 5007)$ is independent of the AGN bolometric luminosity.

To elucidate the possibility of case (1), we compared the distribution of the rest frame $\text{EW}([\text{OIII}]\lambda 5007)$ for two samples (type I ULIRGs and PG QSOs). Figure 3 shows the rest frame $\text{EW}([\text{OIII}]\lambda 5007)$ histogram. Shaded bars represent the distribution of rest frame $\text{EW}([\text{OIII}]\lambda 5007)$ for type I ULIRGs. Unshaded bars denote the distribution of rest frame

EW[O III] λ 5007 for PG QSOs. To investigate whether these two distributions were statistically different, we applied the Kolmogorov-Smirnov statistical test, which has the advantage of making no initial assumption about the distribution of data, with the null hypothesis that the two distributions are from the same parent sample. The Kolmogorov-Smirnov test resulted in a probability of 18.6%, which indicates that the null hypothesis cannot be rejected. This result does not favor case (1).

Thus, the physical origin of the anti-correlation (M_{BH} vs. $L_{\text{IR}}/L_{\text{Edd}}$) is the result of case (2), namely $L_{\text{bol}}/L_{\text{Edd}}$ is anti-correlated with M_{BH} over four orders of magnitude. Bearing in mind that $L_{\text{bol}}/L_{\text{Edd}}$ is a positive function of $\dot{M}_{\text{BH}}/\dot{M}_{\text{Edd}}$, Fig. 2 shows that \dot{M}_{BH} is not proportional to M_{BH} . The absolute value of the mass accretion rate \dot{M}_{BH} can be given by $\dot{M}_{\text{BH}} \sim L_{\text{IR}}/c^2 \approx 0.1M_{\odot}\text{yr}^{-1}(L_{\text{IR}}/10^{12}L_{\odot})$ because of $L_{\text{bol}} = \eta\dot{M}_{\text{BH}}c^2$ and $L_{\text{IR}} = \epsilon L_{\text{bol}}$, where η is assumed to be 0.1–0.42 (the energy conversion efficiency of a BH) and the covering factor of tori ϵ is 0.3–0.5 (e.g., Sanders et al. 1989). Note that the mass accretion rate we estimated here may be underestimated, as $L_{\text{bol}}/L_{\text{Edd}}$ becomes insensitive to $\dot{M}_{\text{BH}}/\dot{M}_{\text{Edd}}$ in the super-critical accretion flows by the photon-trapping effect (e.g., Begelman 1978; Watarai et al. 2000; Ohsuga et al. 2002, 2005). In contrast to this line of reasoning, Begelman (2002) proposed that the maximum AGN bolometric luminosity can exceed AGN Eddington luminosity by a factor of 100 due to photon bubble instability in the radiation pressure-dominated accretion disks. If this is the case, our evaluation might be reasonable.

Moreover, we found that the type I ULIRGs had a higher absolute mass accretion rate than QSOs because the average infrared luminosity of type I ULIRGs was larger than that of QSOs (see Table 4). Thus, we can conclude that the mass accretion process onto a SMBH is regulated by external mechanisms and are not AGN Eddington-limited, which is also the case for type I Seyfert galaxies (Collin & Kawaguchi 2004).

On the basis of these findings (§§4.1 and 4.2), we suggest that a central SMBH grows as its mass accretion rate changes from super-Eddington to sub-Eddington along an evolutionary track (type I ULIRG \rightarrow NLQSO \rightarrow BLQSO).

5. Discussion and Conclusions

To reveal how a SMBH grows in the evolutionary track from ULIRG into QSO, we investigated the relationship between SMBH mass and infrared luminosity, which is a good tracer of AGN activities for type I ULIRGs. Our main conclusions are the following:

1. We discovered the anti-correlation between the mass of a SMBH (M_{BH}) and the ratio of infrared to AGN Eddington luminosity ($L_{\text{IR}}/L_{\text{Edd}}$) over four orders of magnitude for

type I ULIRGs and QSOs, $\log(L_{\text{IR}}/L_{\text{Edd}}) = -0.961(\pm 0.081) \log M_{\text{BH}} + 7.06(\pm 0.65)$. In the case of BLQSOs only, the slope in the M_{BH} vs. $L_{\text{IR}}/L_{\text{Edd}}$ diagram was shallower than those of the other targets,

2. Type I ULIRGs and QSOs have the same distribution of the rest frame EW([OIII] λ 5007). Because the rest frame EW([OIII] λ 5007) mirrors the geometry of the obscuring torus, the anti-correlation (M_{BH} vs. $L_{\text{IR}}/L_{\text{Edd}}$) can be explained as the anti-correlation between the mass of a SMBH and the mass accretion rate onto a SMBH normalized by that of the AGN Eddington. That is to say, the mass accretion rate \dot{M}_{BH} is not proportional to the mass of a SMBH. Furthermore, type I ULIRGs with smaller BHs tend to show higher mass accretion rates than QSOs. Hence, the anti-correlation indicates that the SMBH growth process is regulated by external mechanisms rather than the self-regulation of an accretion disk around a central BH.
3. Super-Eddington mass accretion flow is a characteristic of type I ULIRGs ($\approx 85\%$ in our sample) because the infrared luminosity is greater than the AGN Eddington luminosity. However, all BLQSOs showed that the ratio of infrared to AGN Eddington luminosity was less than unity, which indicates a sub-Eddington mass accretion rate. It is also interesting that for three NLQSOs with hard X-ray power-law photon index $\Gamma_{2-10\text{keV}} > 2$, the mass accretion rate \dot{M}_{BH} was between that of type I ULIRGs and BLQSOs.
4. Based on all of these findings (1-3), we propose an evolutionary track (type I ULIRG \rightarrow NLQSO \rightarrow BLQSO) altering the mass accretion rate from super-Eddington to sub-Eddington.

Finally, it is worth discussing the physical reason for the anti-correlation M_{BH} vs. $L_{\text{IR}}/L_{\text{Edd}}$. Based on a coevolutionary model of SMBHs and spheroidal galaxies (KUM03; see also Granato et al. 2004) that takes into account angular momentum extraction via radiation drag (Umemura 2001; Kawakatu & Umemura 2002; Sato et al. 2004), massive tori form in the early phase of BH growth like type I ULIRGs, which are accreted onto SMBHs only at the last e -folding time ($t_e = 4 \times 10^7 \text{yr}$). Thus, the mass ratio of a massive torus to a SMBH, $M_{\text{torus}}/M_{\text{BH}}$, would be much larger than unity for type I ULIRGs, whereas $M_{\text{torus}}/M_{\text{BH}}$ would be less than unity for QSOs. Typical length scales (r_{torus}) of such tori can be estimated as $r_{\text{torus}}/100 \text{pc} \sim 0.44\alpha M_8/v_{100}^2$, where M_8 is the BH plus the torus mass in $10^8 M_{\odot}$ and v_{100} is the velocity in 100 km/s. The factor α can be inferred by high resolution-observations of tori in nearby AGN (e.g., Jaffe et al. 1993; van der Marel et al. 1998; Davis et al. 2006) and turns out to be at least a few $\alpha \sim$. According to KUM03, the dust emission from massive tori in type I ULIRGs is cooler than that in QSOs because of the higher column density

of massive tori. This coincides with observational data indicating that the average infrared color (f_{25}/f_{60}) of type I ULIRGs is cooler than that of QSOs, as shown in Table 4.

In such a massive torus, the viscosity works effectively because the timescale for viscous accretion is proportional to its specific angular momentum, which can be reduced by radiation drag. Thus, a massive torus is likely to be a self-gravitating viscous object (e.g., Umemura 2004; Kawakatu & Umemura 2005; and references therein). As a plausible process of mass accretion onto a central BH, we consider the turbulent viscous drag whose timescale is $t_{\text{vis}} \sim r^2/\nu$, where r is the distance from galactic nuclei and ν is the viscous coefficient. Here we adopt $\nu = R_{\text{crit}}^{-1} r v_{\phi}$, where $R_{\text{crit}} = 100 - 1000$ and v_{ϕ} are the critical Reynolds numbers for the onset of turbulence (e.g., Duschl et al. 2000; Burkert & Silk 2001) and the rotation velocity, respectively. Then, the viscous time can be given by $t_{\text{vis}} = R_{\text{crit}} t_{\text{dyn}}$, where the dynamical timescale should be determined by the central BH plus a surrounding massive torus system. As a consequence, the mass accretion rate (\dot{M}_{BH}) via the viscous drag is given as $\dot{M}_{\text{BH}} \propto (M_{\text{torus}}/M_{\text{BH}})^{3/2} [1 + (M_{\text{BH}}/M_{\text{torus}})]^{-1/2}$ [see also eq. (22) in Granato et al. 2004]. Combining their prediction (KUM03) and mass accretion process due to the turbulent viscous drag, the anti-correlation M_{BH} vs. $L_{\text{IR}}/L_{\text{Edd}}$ (or $L_{\text{bol}}/L_{\text{Edd}}$) can be explained. If this interpretation is correct, the rate of mass accretion onto a BH may depend on the mass ratio, $M_{\text{torus}}/M_{\text{BH}}$. In other words, the onset of super-Eddington mass accretion may be linked to the presence of a massive torus around a central BH. To test this postulate, it will be crucial to detect massive tori among type I ULIRGs with super-Eddington mass accretion flows through carbon monoxide and hydrogen cyanide molecular emission (see also Kawakatu et al. 2007). To resolve ~ 100 pc massive tori at the typical redshift of type I ULIRGs $z \approx 0.2$, use of the Atacama Large Millimeter Array instrument is essential because a resolution of $\approx 0.1''$ would be necessary.

Starburst activity around AGNs may also be a key ingredient in interpreting the anti-correlation (M_{BH} vs. $L_{\text{IR}}/L_{\text{Edd}}$), as the starburst leads to an effective mass accretion onto a central SMBH (e.g., Norman & Scoville 1988; Umemura et al. 1997; Wada & Norman 2002). If this is the case, the galaxies with super-Eddington mass accretion will have larger starburst luminosity than those with sub-Eddington mass accretion. Scientists will be able to check this trend by comparing the PAH luminosity in type I ULIRGs with that in PG QSOs.

Therefore, to reveal the key physics that theoretically control mass accretion onto a central BH, it is necessary to determine the mass accretion rate via turbulent viscous drag and other physical mechanisms connected to starburst phenomena from a massive torus to a central BH with sophisticated numerical simulations. We leave this challenge for the future.

We thank an anonymous reviewer for constructive suggestions. N. K. thanks K. Wada for useful and stimulating discussions. M. I. is supported by Grants-in-Aid for Scientific Research (16740117). T. N. acknowledges financial support from the Japan Society for the Promotion of Science (JSPS) through the JSPS Research Fellows. This study made use of the NASA/IPAC Extragalactic Database (NED) operated by the Jet Propulsion Laboratory, California Institute of Technology, under contract with the National Aeronautics and Space Administration.

REFERENCES

- Abramowicz, M. A., et al. 1988, *ApJ*, 332, 646
- Bahcall, J. N., et al. 1997, *ApJ*, 479, 642
- Barger, A. J., et al. 2005, *AJ*, 129, 578
- Begelman, M. C. 1978, *MNRAS*, 184, 53
- Begelman, M. C. 2002, *ApJ*, 568, L97
- Bentz, M. C., et al. 2006, *ApJ*, in press (astro-ph/0602412)
- Boller, Th., Brandt, W. N., & Fink, H. 1996, *A&A*, 305, 53 Boroson, T. A., & Green, R. F., 1992, *ApJS*, 80, 109
- Bryant, P. M., & Scoville, N. Z. 1999, *AJ*, 117, 2632
- Burkert, A., & Silk, J. 2001, *ApJ*, 554, L151
- Canalizo, G., & Stockton, A., 2001, *ApJ*, 555, 719
- Collin, S., & Kawaguchi, T. 2004, *A&A*, 426, 797
- Davis, R. I., et al. 2006, *ApJ*, in press (astro-ph/0604125)
- de Grijp, M. H. K., Miley, G. K., & Lub, J. 1987, *A&A*, 70, 95
- Downes, D., & Solomon, P. M. 1998, *ApJ*, 507, 615
- Dunlop, S. et al. 2003, *MNRAS*, 340, 1095
- Duschl, W. J., Strittmatter, P. A., & Biermann, P. L. 2000, *A&A*, 357, 1123 Ferrarese, L., & Merritt, D. 2000, *ApJ*, 539, L9

- Fischer, J. 2000, in *ISO Beyond the Peaks*, ed. A. Salama et al. (ESA SP-456; Noordwijk: ESA), 239
- Gao, Y., & Solomon, P.-M. 2004, *ApJ*, 606, 271
- Genzel, R., et al. 2001, *ApJ*, 563, 527
- Granato, G. L., et al. 2004, *ApJ*, 600, 580
- Haas, M., et al. 2000, *A&A*, 354, 453
- Haas, M., et al. 2003, *A&A*, 402, 87
- Hao, C. N., et al. 2005, *ApJ*, 625, 76
- Ho, L. 2005, *ApJ*, 629, 680
- Imanishi, M. 2002, *ApJ*, 569, 44
- Imanishi, M., 2006, *AJ*, 131, 2406
- Imanishi, M., Dudley, C. C., & Maloney, P. R. 2006b, *ApJ*, 637, 114
- Imanishi, M., Nakanishi, K., & Kohno, K. 2006a, *AJ*, 131, 2888
- Iye, M. et al., 2004, *PASJ*, 56, 381
- Jaffe, W., et al. 1993, *Nature*, 364, 213
- Kaspi, S., et al. 2000, *ApJ*, 533, 631
- Kawaguchi, T. 2003, *ApJ*, 593, 69
- Kawakatu, N., & Umemura, M. 2002, *MNRAS*, 329, 572
- Kawakatu, N., & Umemura, M. 2004, *ApJL*, 601, L21
- Kawakatu, N., & Umemura, M. 2005, *ApJ*, 628, 721
- Kawakatu, N., Umemura, M., & Mori, M. 2003, *ApJ*, 583, 85
- Kawakatu, N., Anabuki, N., Nagao, T., Umemura, M., & Nakagawa, T. 2006, *ApJ*, 637, 104
- Kawakatu, N., Andreani, P., Granato, G. L. & Danese, L., 2007, *ApJ*, submitted
- Kellerman, K. I., et al. 1989, *AJ*, 98, 1195

- Kim, D.-C., & Sanders, D. B. 1998, *ApJS*, 119, 41
- Kobayashi, N., et al. 2000, IRCS: Infrared camera and spectrograph for the Subaru Telescope, in *Proc. SPIE 4008: Optical and IR Telescope Instrumentation and Detectors*, eds M. Iye & A. F. Moorwood, 1056
- Kormendy, J., & Richstone, D. 1995, *ARA&A*, 33, 581
- Kormendy, J., & Sanders, D. B. 1992, *ApJ*, 388, L9
- Laor, A. 1998, *ApJ*, 505, L83
- Lawrence, A., et al. 1999, *MNRAS*, 308, 897
- Lutz, D., Veilleux, S., & Genzel, R. 1999, *ApJ*, 517, L13
- Magorrian, J., et al. 1998, *AJ*, 115, 2285
- Marconi, A., & Hunt, L. K. 2003, 589, L21
- Marconi, A., Risaliti, G., Gilli, R., Hunt, L. K., Maiolino, R., & Salvati, M. 2004, *MNRAS*, 351, 169
- Marziani, P., et al. 2003, *MNRAS*, 345, 1133
- McLeod, K. K., & Rieke, G. H. 1995, *ApJ*, 454, L77
- McLeod, K. K., Rieke, G. H., & Storrie-Lombardi, L. J. 1999, *ApJ*, 511, L6
- McLure, R. J., & Dunlop, J. S. 2001, *MNRAS*, 327, 199
- McLure, R. J., & Dunlop, J. S. 2002, *MNRAS*, 331, 795
- McLure, R. J., Dunlop, J. S., & Kukula, M. J. 2000, *MNRAS*, 318, 693
- Mineshige, S., Kawaguchi, T., Takeuchi, M., & Hayashida, K. 2000, *PASJ*, 52, 499
- Moran, E. C., Halpern, J. P., & Helfand, D., J. 1996, *ApJ*, 106, 341
- Mouri, H., Kawara, K., Taniguchi, Y., & Nishida, M. 1990, *ApJ*, 356, L39
- Neugebauer, G., et al. 1987, *ApJS*, 63, 615
- Norman, C., & Scoville, N. 1988, *ApJ*, 332, 124
- Ohsuga, K., Mori, M., Nakamoto, T., & Mineshige, S. 2005, *ApJ*, 628, 368

- Ohsuga, L., Mineshige, S., Mori, M., & Umemura, M. 2002, *ApJ*, 574, 315
- Peterson, B. M., & Wandel, A. 1999, *ApJ*, 521, L95
- Peterson, B. M., & Wandel, A. 2000, *ApJ*, 540, L13
- Peterson, B. M., et al. 2000, *NewAR*, 44, 491
- Piconcelli, E., et al. 2005, *A&A*, 432, 15
- Pound, K. A., Done, C., & Osbore, J. P. 1995, *MNRAS*, 277, L5
- Richstone, D., et al. 1998, *Nature*, 395A, 14
- Rieke, G. H., & Lebofsky, M. J. 1985, *ApJ*, 288, 6
- Rowan-Robinson, M. 1995, *MNRAS*, 272, 737
- Sanders, D. B., & Mirabel, I. F. 1996, *ARA&A*, 34, 749
- Sanders, D. B., et al. 1988, *ApJ*, 325, 74
- Sanders, D. B., et al. 1989, *ApJ*, 347, 29
- Sato, J., et al. 2004, *MNRAS*, 354, 176
- Schmidt, M., & Green, R. F. 1983, *ApJ*, 269, 352
- Schweitzer, M., et al. 2006, *ApJ*, in press (astro-ph/0606158)
- Shemmer, O., et al. 2004, *ApJ*, 614, 547
- Shemmer, O., Brandt, W. N., Netzer, H., Maiolino, R., Kaspi, S., 2006, in press (astro-ph/0606389)
- Tacconi, L. J., et al. 2002, *ApJ*, 580, 73
- Teng, S. H., et al. 2005, *ApJ*, 633, 664
- Tokunaga, A. T. 2000, in *Allen's Astrophysical Quantities*, ed. A. N. Cox (4th ed; Berlin: Springer), 143
- Tokunaga, A. T., Sellgren, K., Smith, R. G., Nagata, T., Sakata, A., & Nakada, Y. 1991, *ApJ*, 380, 452
- Tremaine, S., et al. 2002, *ApJ*, 574, 740

- Umemura, M. 2001, *ApJ*, 560, L29
- Umemura, M., 2004, in *Coevolution of Black holes and Galaxies*, ed. L. C. Ho (Pasadena: Carnegie Observatories, <http://www.ociw.edu/ociw/symposia/series/symposium1/proceedings.html>)
- Umemura, M., Fukue, J., & Mineshige, S. 1997, *ApJ*, 479, L97
- van der Marel, R. P., et al. 1998, *AJ*, 116, 2220
- Veilleux, S., Sanders, D. B., & Kim, D.-C. 1999, *ApJ*, 522, 139
- Veilleux, S., Kim, D.-C., & Sanders, D. B. 2002, *ApJS*, 143, 315
- Veilleux, S, et al. 2006, *ApJ*, in press (astro-ph/0601565)
- Voit, G.-M. 1992, *MNRAS*, 258, 841
- Wada, K., & Norman, C. A., *ApJ*, 2002, 566, L21
- Wang, J., Szuskiewicz, E., Lu, F., & Zhou, Y 1999, *ApJ*, 522, 839
- Wang, T. G., & Lu, Y. J. 2001, *A&A*, 377, 52
- Watarai, K., Fukue, J., Takeuchi, M., & Mineshige, S. 2000, *PASJ*, 52, 133
- Zheng, X., Xia, X., Mao, S., Wu, H., & Deng, Z. G. 2002, *AJ*, 124, 18

A. Infrared L -band spectra of two type I ULIRG nuclei

Observations of IRAS 16136+6550 and 22454–1744 were made on 19 and 20 July 2006 (UT), respectively, using a IRCS near-infrared spectrograph (Kobayashi et al. 2000) attached to a Nasmyth focus of a Subaru 8.2-m telescope (Iye et al. 2004). The sky was clear and the observation at K , measured in images taken before L -band spectroscopy, was $\sim 0''.5$ in full-width at half-maximum. A $0''.6$ -wide slit and the L -grism were used with a 52-mas pixel scale. The achievable spectral resolution is $R \sim 140$ at $\lambda \sim 3.5 \mu\text{m}$. A standard telescope nodding technique (ABBA pattern) with a throw of 5 to $7''$ along the slit was employed to subtract background emission. The optical guider of the Subaru telescope was used to monitor the telescope tracking. Exposure time was 1.2 s, and 50 coadds were made at each nod position. The total net on-source integration times were 16 min for both sources.

HR 6360 (G5V, $V=6.10$) and HR 8544 (G2V, $V=6.57$) were observed as standard stars, with an airmass difference of < 0.1 for IRAS 16136+6550 and 22454–1744, respectively, to correct for the transmission of the Earth’s atmosphere. The magnitudes of HR 6360 and HR 8544 were estimated to be $L = 4.5$ and $L = 5.1$, respectively, based on their V -band ($0.6 \mu\text{m}$) magnitudes and $V-L$ colors of the corresponding stellar types (Tokunaga 2000).

Standard data analysis procedures were employed using IRAF³. Initially, frames taken with an A (or B) beam were subtracted from frames subsequently taken with a B (or A) beam, and the resulting subtracted frames were added and divided by a spectroscopic flat image. Then, bad pixels and pixels hit by cosmic rays were replaced with the interpolated values of the surrounding pixels. Finally, the spectra of ULIRG nuclei and standard stars were extracted by integrating signals over $0''.6$ to $1''.5$, depending on actual signal profiles. Wavelength calibration was performed taking into account the wavelength-dependent transmission of the Earth’s atmosphere. The spectra of ULIRG nuclei were divided by the observed spectra of standard stars and multiplied by the spectra of blackbodies with temperatures appropriate to individual standard stars ($T = 5700$ K and 5830 K for HR 6360 and HR 8544, respectively).

Flux calibration was done based on signals of ULIRGs and standard stars detected inside our slit spectra. To obtain an adequate signal-to-noise ratio in each element, appropriate binning of spectral elements was performed, particularly at $\lambda_{\text{obs}} < 3.3 \mu\text{m}$ and $> 3.9 \mu\text{m}$ in the observed frame, where the scatter is higher than at $\lambda_{\text{obs}} = 3.3\text{--}3.9 \mu\text{m}$ due to the Earth’s atmosphere.

³IRAF is distributed by the National Optical Astronomy Observatories operated by the Association of Universities for Research in Astronomy, Inc., under a cooperative agreement with the National Science Foundation.

Both sources showed flux excesses at $\lambda_{\text{obs}} = (1 + z) \times 3.29 \mu\text{m}$, the wavelength at which the 3.3- μm PAH emission feature peaks. We thus identified these features as the 3.3- μm PAH emission in Fig. 4. To estimate the strength of the 3.3- μm PAH emission feature, we adopted a template spectral shape for the Galactic star-forming regions and nearby starburst galaxies (type-1 sources; Tokunaga et al. 1991) as we did previously for other ULIRGs (Imanishi et al. 2006b; Imanishi 2006). The estimated 3.3- μm PAH fluxes were $F(3.3\text{PAH}) \sim 2.0 \times 10^{-14}$ and 4.5×10^{-15} ergs s $^{-1}$ cm $^{-2}$ for IRAS 16136+6550 and 22454–1744, respectively.

Table 1. Infrared Properties of Type I ULIRGs and PG QSOs

Name	z	$\log(\frac{L_{12}}{L_{\odot}})$	$\log(\frac{L_{25}}{L_{\odot}})$	$\log(\frac{L_{60}}{L_{\odot}})$	$\log(\frac{L_{100}}{L_{\odot}})$	$\log(\frac{L_{IR}}{L_{\odot}})$	$\frac{f(25)}{f(60)}$	References
(1)	(2)	(3)	(4)	(5)	(6)	(7)	(8)	(9)
Type I ULIRGs								
F00275–2859	0.279	<11.96	11.96	12.18	11.99	12.56	0.25(w)	1
F01572+0009(Mrk 1014)	0.163	11.69	11.95	12.23	12.00	12.53 (11.7)	0.22(w)	1,3
F02054+0835	0.345	12.49	<12.29	12.29	12.62	12.95	< 0.42	1
F02065+4705	0.132	<11.42	11.33	11.69	11.81	12.10	0.18(c)	1
F04416+1215	0.089	<11.41	11.37	11.66	11.52	12.02	0.21(w)	1
IR 06269–0543	0.117	11.62	11.91	12.05	11.79	12.39	0.30(w)	1
F07598+6508	0.148	11.89	11.88	12.00	11.79	12.42 (< 12.0)	0.32(w)	1,3
F09427+1929	0.284	12.06	<11.92	12.05	12.14	12.56	< 0.30	1
F10026+4347	0.178	<11.74	11.58	11.68	11.66	12.19	0.33(w)	1
F11119+3257	0.189	11.91	11.91	12.19	11.95	12.54	0.22(w)	1
Z11598–0112	0.151	<12.04	<11.90	12.17	12.00	12.56 (11.3)	< 0.22	1,3
F12134+5459	0.150	<11.38	11.17	11.59	11.71	12.01	0.16(c)	1
F12265+0219 (3C 273)	0.158	12.15	12.18	12.08	12.10	12.65 (< 12.0)	0.52(w)	1,3
F12540+5708 (Mrk 231)	0.042	11.64	11.98	12.20	11.94	12.50 (11.2)	0.25(w)	1,3
F13342+3932	0.179	<11.72	<11.72	11.99	11.93	12.37	< 0.22	1
F15069+1808	0.171	<11.56	11.36	11.73	11.69	12.12	0.17(c)	1
F15462–0450	0.101	<11.23	11.46	11.89	11.68	12.15 (11.3)	0.16(c)	1,3
F16136+6550	0.129	11.28	11.39	11.45	11.46	11.91 (11.1)	0.36(w)	1,3
F18216+6419	0.297	12.48	12.43	12.50	12.51	13.00	0.36(w)	1
F20036–1547	0.193	<11.81	<11.84	12.23	12.08	12.54	< 0.17	1
F20520–2329	0.206	<11.87	<11.68	11.97	12.03	12.42	< 0.21	1
F21219–1757	0.113	11.54	11.56	11.56	11.38	12.04 (10.7)	0.42(w)	1,3
F22454–1744	0.117	<11.67	11.39	11.46	11.33	12.02 (10.3)	0.36(w)	1,3
PG QSOs								
PG 0003+158	0.450	<12.05	<12.11	<11.62	<11.85	<12.47	<-1.28	1
PG 0007+106 (III Zw 2)	0.089	11.01	10.91	10.64	<11.02	11.05	0.76	2
PG 0026+129	0.142	<10.69	<10.71	<10.16	<10.41	<11.07	<1.48	1
PG 0043+039	0.384	<12.32	<12.19	<11.78	<11.87	<12.63	<1.06	1
PG 0050+124 (IZw 1)	0.061	11.42	11.40	11.34	11.23	11.88	0.48	1
PG 0052+251	0.155	<11.41	<11.45	<10.78	11.12	11.78	<1.95	1
PG 0804+761	0.100	11.23	11.14	10.69	10.28	11.52	1.14	2
PG 0838+770	0.131	10.89	11.05	10.90	11.07	11.49	0.59	1
PG 0844+349 (Ton 951)	0.064	10.82	10.71	10.24	10.27	11.12	1.25	1
PG 0923+201	0.190	<11.68	<11.56	<11.47	<11.77	<12.14	<0.5	1
PG 0953+414	0.239	<11.85	< 11.61	<11.31	<11.48	<12.14	<0.83	1
PG 1004+130	0.240	<11.87	11.76	11.49	<11.44	11.87 — 12.21	0.78	1
PG 1012+008	0.185	<11.70	<11.52	<11.12	<11.29	<11.99	1.05	1
PG 1049–005	0.357	12.23	12.21	11.86	<11.97	12.62	0.10	1
PG 1100+772 (3C 249.1)	0.313	11.41	11.44	11.23	10.83	11.82	0.73	2
PG 1103–006	0.425	<12.51	<12.31	11.86	<12.11	11.83 — 12.79	<1.17	1
PG 1114+445	0.144	11.38	11.29	<11.12	10.82	11.74	0.78	2
PG 1116+215 (Ton 1388)	0.177	11.81	11.58	<11.27	<11.16	12.07	>0.85	2
PG 1119+120 (Mrk 734)	0.049	10.57	10.62	10.52	10.44	11.07	0.51	1
PG 1149–110	0.049	10.57	10.60	10.35	10.06	10.98	0.74	2
PG 1202+281	0.165	<11.56	11.34	10.91	<11.27	11.56 — 11.85	>1.13	1

Table 1. - Continued

Name (1)	z (2)	$\log(\frac{L_{12}}{L_{\odot}})$ (3)	$\log(\frac{L_{25}}{L_{\odot}})$ (4)	$\log(\frac{L_{60}}{L_{\odot}})$ (5)	$\log(\frac{L_{100}}{L_{\odot}})$ (6)	$\log(\frac{L_{IR}}{L_{\odot}})$ (7)	$\frac{f(25)}{f(60)}$ (8)	References (9)
PG 1229+204 (Mrk771)	0.064	10.56	10.60	10.40	<10.30	11.20	1.94	1
PG 1244+026	0.048	10.40	10.46	10.34	10.11	10.87	0.56	2
PG 1259+593	0.472	<12.59	<12.30	<12.03	<12.16	<12.86	<0.78	1
PG 1302-102	0.286	<12.14	<12.01	<11.59	<11.76	12.46	<1.07	1
PG 1307+085	0.155	<11.56	<11.38	<11.00	<11.13	11.86	<0.94	1
PG 1309+355 (Ton 1565)	0.184	11.44	11.35	<11.18	<11.03	11.65 — 11.81	>0.63	2
PG 1322+659	0.168	11.44	11.039	10.83	11.07	11.47	0.6	2
PG 1351+236	0.055	<10.61	<10.32	10.45	10.29	10.99 — 11.38	<0.31	1
PG 1351+640	0.087	11.12	11.42	11.15	10.79	11.29	0.76	2
PG 1352+183	0.158	<11.55	<11.26	<10.97	<11.15	11.22	<0.81	2
PG 1354+213	0.300	<12.13	<11.85	< 11.60	<11.73	<12.41	<0.73	1
PG 1402+261	0.164	11.40	11.32	11.18	10.97	11.81	0.52	1
PG 1411+442	0.089	11.07	10.90	10.52	10.34	11.34	0.99	1
PG 1415+451	0.114	10.88	10.77	10.58	10.48	11.24	0.65	2
PG 1416-129	0.129	<11.38	<11.28	< 10.79	<10.92	<11.69	<1.29	1
PG 1425+267	0.366	<12.27	< 11.91	<11.66	<11.88	<12.52	<0.74	1
PG 1426+015 (Mrk 1383)	0.086	11.081	10.90	10.79	< 10.56	11.39	0.54	2
PG 1427+480	0.221	11.66	11.33	11.14	11.27	11.93	0.58	2
PG 1435-067	0.129	11.33	<11.21	10.75	<10.92	11.59	<0.41	2
PG 1440+356 (Mrk478)	0.077	10.99	10.89	10.96	10.86	11.46	0.35	2
PG 1444+407	0.267	11.78	11.72	11.40	10.99	12.11	0.86	2
PG 1501+106 (Mrk 841)	0.036	10.25	10.53	10.20	<9.75	10.79	0.89	1
PG 1512+370 (4C37.43)	0.371	11.87	11.69	11.43	<11.32	12.17	0.77	1
PG 1519+226	0.137	11.26	10.94	<10.75	<10.88	11.51	>0.57	2
PG 1534+580 (Mrk 290)	0.030	10.057	10.00	9.56	9.61	10.39	1.13	1
PG 1545+210 (3C323.1)	0.266	11.40	11.32	10.96	10.56	11.71	0.96	2
PG 1612+261	0.131	<10.88	<10.64	<10.39	<10.64	<11.19	<0.96	1
PG 1613+658(Mrk876)	0.129	11.28	11.39	11.45	11.46	11.91	0.36	1
PG 1626+554	0.133	10.95	10.64	<10.52	10.83	11.33	>0.32	2
PG 1704+608 (3C 351)	0.371	12.01	12.04	11.92	11.57	12.46	0.53	2
PG 2112+059	0.466	12.38	12.07	11.85	<11.86	12.64	0.69	1
PG 2130+099 (II Zw 136)	0.061	10.95	10.88	10.66	10.44	11.32	0.69	2
PG 2251+113	0.323	<11.74	<11.68	<11.31	<11.59	<12.13	0.98	1
PG 2308+098 (4C 09.72)	0.432	11.76	11.89	<12.01	<11.75	12.07 — 12.39	>0.31	2
PG 2349-014	0.173	<11.69	<11.55	11.35	11.16	11.47 — 12.02	<0.66	1

Note.-Col. (1): Source name. Col. (2): Redshift. Cols. (3-6): L_{12} , L_{25} , L_{60} , and L_{100} are the monochromatic luminosities (νL_{ν}) at $12\mu\text{m}$, $25\mu\text{m}$, $60\mu\text{m}$, and $100\mu\text{m}$, respectively. Col. (7): Infrared luminosity and the values in parentheses are infrared luminosity due to starburst, $\log(\frac{L_{IR(SB)}}{L_{\odot}})$, which was derived by $L_{3.3PAH}/L_{IR(SB)} = 10^{-3}$ for starburst-dominated galaxies (e.g., Mouri et al. 1990; Imanishi 2002). Polycyclic aromatic hydrocarbon luminosity was based on Imanishi et al. (2006b) and recent observations (see Appendix). Col. (8): Ultraluminous infrared galaxies with type I Seyfert nuclei (type I ULIRGs) with $f(25)/f(60) < 0.2$ and > 0.2 are classified as cool and warm (represented as C and W, respectively; Sanders et al. 1988). Col. (9): References.-(1) Sanders et al. (1989); (2) Haas et al. (2003); (3) Imanishi et al. (2006b).

Table 2. Variable Physical Parameters for Ultraluminous Infrared Galaxies With Type I Seyfert Nuclei

Name	$\log(\frac{M_{\text{BH}}}{M_{\odot}})$	$\log(\frac{L_{\text{IR.}}}{L_{\text{Edd}}})$	EW[O III](Å)	References
(1)	(2)	(3)	(4)	(5)
F00275–2859	7.27	0.78	10.7	1
F01572+0009(Mrk 1014) ^a	7.87	0.15	45.8	1
F02054+0835	7.68	0.76	9.2	1
F02065+4705	6.89	0.69	13.6	1
F04416+1215	6.66	0.85	28.0	1
IR 06269–0543	6.93	0.95	85.2	1
F07598+6508	8.17	-0.26	<1.1	1
F09427+1929	7.50	0.55	<1.1	1
F10026+4347	7.54	0.14	3.8	1
F11119+3257	7.24	0.79	38.5	1
Z11598–0112 ^a	6.36	1.69	10.5	1
F12134+5459	6.10	1.40	22.8	1
F12265+0219 (3C 273)	9.00	-0.86	4.9	1
F12540+5708 (Mrk 231)	7.94	0.05	<4.1	1
F13342+3932	6.58	1.28	38.0	1
F15069+1808	6.92	0.71	47.2	1
F15462–0450	6.31	1.33	32.2	1
F16136+6550	8.70	-1.30	11.7	1
F18216+6419	9.13	-0.64	22.9	1
F20036–1547	7.32	0.71	<0.3	1
F20520–2329	7.15	0.79	10.3	1
F21219–1757	7.15	0.38	11.2	1
F22454–1744	6.32	1.19	35.8	1

Note.-Col. (1): Source name. Col. (2): Black hole mass. Col. (3): $L_{\text{IR}}/L_{\text{Edd}}$. Col. (4): Equivalent width of [O III] λ 5007Å at the rest frame. Col. (5): References (for cols. [2] and [4]).

References.-(1) Zheng et al. (2002).

The symbol *a*: Object showed a soft X-ray excess and a steep photon index $\Gamma_{2-10\text{keV}} > 2$ (Teng et al. 2002).

Table 3. Variable Physical Parameters for PG QSOs

Name	$\log(\frac{M_{\text{BH}}}{M_{\odot}})$	$\log(\frac{L_{\text{IR}}}{L_{\text{Edd}}})$	EW[O III](Å)	References
(1)	(2)	(3)	(4)	(5)
PG 0003+158	9.34	<-1.38	26	(2&4),2
PG 0007+106 (III Zw 2)	8.29	-1.75	42	(2&3),2
PG 0026+129	7.85	<-1.29	29	(2&3),2
PG 0043+039	9.23	<-1.11	1	(2&3),2
PG 0050+124 (IZw 1) ^a	7.26	0.11	22	(2&4),2
PG 0052+251	8.72	-1.45	30	(2&3),2
PG 0804+761	8.31	-1.30	9	(2&3),2
PG 0838+770	7.99	-1.01	13	(2&3),2
PG 0844+349 (Ton 951)	7.69	-1.08	8	(2&3),2
PG 0923+201	8.95	<-1.32	7	1,2
PG 0953+414	8.58	<-0.95	18	(2&3),2
PG 1004+130	9.11	-1.75 — -1.41	6	1,2
PG 1012+008	7.80	<-0.32	29	1,2
PG 1049-005	9.14	-1.03	55	(2&3),2
PG 1100+772 (3C 249.1)	9.07	-1.76	41	(2&3),2
PG 1103-006	9.29	-1.97 — -1.01	8	(2&3),2
PG 1114+445	8.41	-1.18	14	(2&3),2
PG 1116+215 (Ton 1388)	8.22	-0.66	10	1,2
PG 1119+120 (Mrk 734)	7.20	-0.64	19	(2&3),2
PG 1149-110	7.57	-1.10	33	(2&3),2
PG 1202+281	8.30	-1.25 — -0.96	36	1,2
PG 1211+143 ^b	7.88	-0.81	12	(2&3),2
PG 1216+069	9.17	-1.35	10	(2&3),2
PG 1229+204 (Mrk771)	7.93	-1.24	19	(2&3),2
PG 1244+026 ^a	6.29	0.07	17	(2&3),2
PG 1259+593	8.98	<-0.63	0	(2&3),2
PG 1302-102	8.31	-0.8 — -0.36	9	1,2
PG 1307+085	7.86	-1.15 — -0.51	32	1,2
PG 1309+355 (Ton 1565)	8.21	-1.07 — -0.91	19	(2&3),2
PG 1322+659	8.16	-1.20	8	(2&3),2
PG 1351+236	8.31	-1.83 — -1.44	12	(2&3),2
PG 1351+640	8.69	-1.91	12	(2&3),2
PG 1352+183	8.27	-1.56	10	(2&3),2
PG 1354+213	8.54	<-0.64	31	(2&3),2
PG 1402+261 ^a	7.30	0.0	1	1,2
PG 1411+442	7.89	-1.06	15	(2&3),2
PG 1415+451	7.81	-1.08	1	(2&3),2
PG 1416-129	8.50	<-1.32	49	(2&3),2
PG 1425+267	9.78	<-1.77	36	(2&3),2
PG 1426+015 (Mrk 1383)	8.75	-1.87	11	(2&3),2
PG 1427+480	8.00	-0.58	58	(2&3),2

Table 3. - Continued

Name	$\log(\frac{M_{\text{BH}}}{M_{\odot}})$	$\log(\frac{L_{\text{IR}}}{L_{\text{Edd}}})$	EW[O III](Å)	References
(1)	(2)	(3)	(4)	(5)
PG 1435–067	8.24	–1.16	12	(2&3),2
PG 1440+356 (Mrk478) ^b	7.30	–0.35	10	(2&3),2
PG 1444+407	8.23	–0.63	1	(2&3),2
PG 1501+106 (Mrk 841)	7.88	–1.60	64	(2&3),2
PG 1512+370 (4C37.43)	8.95	–1.29	57	(2&3),2
PG 1519+226	7.78	–0.78	4	(2&3),2
PG 1534+580 (Mrk 290)	7.36	–1.48	79	(2&3),2
PG 1545+210 (3C323.1)	8.94	–1.74	33	1,2
PG 1612+261	7.91	<–1.23	157	(2&3),2
PG 1613+658(Mrk876)	8.99	–1.59	20	(2&3),2
PG 1626+554	8.36	–1.54	9	(2&3),2
PG 1704+608 (3C 351)	7.88	0.07	27	(2&3),2
PG 2112+059	9.14	–1.01	0	(2&3),2
PG 2130+099 (II Zw 136)	7.68	–0.87	20	(2&3),2
PG 2251+113	8.96	<–1.34	19	(2&3),2
PG 2308+098 (4C 09.72)	9.57	–2.01 — –1.69	17	(2&4),2
PG 2349–014	8.79	–1.83 — –1.28	—	1,2

Note.-Col. (1): Source name. Col. (2): Black hole mass. Col. (3): $L_{\text{IR}}/L_{\text{Edd}}$. Col. (4): Equivalent width of [O III] λ 5007Å at the rest frame. Col. (5): References (for cols. [2] and [4], respectively).

References.-(1) McLure & Dunlop (2001) for the full width at half maximum [FWHM(H β)] and the $L_{\lambda}(5100\text{Å})_{\text{rest}}$; (2) Boroson & Green (1992) for the FWHM(H β); (3) Neugebauer et al. (1987) for the $L_{\lambda}(5100\text{Å})_{\text{rest}}$; (4) Schmidt & Green (1983) for the $L_{\lambda}(5100\text{Å})_{\text{rest}}$.

Underlined objects are narrow-line QSOs whose FWHMs of the broad H β lines were less than 2000 km/s.

The symbol *a*: Object showed a steep hard X-ray photon index $\Gamma_{2-10\text{keV}} > 2$. The symbol *b*: Hard X-ray photon index $\Gamma_{2-10\text{keV}} < 2$ (Piconcelli et al. 2005).

Table 4. Comparison of Several Physical Properties

Name	$\langle \log(\frac{L_{\text{IR}}}{L_{\odot}}) \rangle$	$\langle \log(\frac{M_{\text{BH}}}{M_{\odot}}) \rangle$	$\langle \log(\frac{L_{\text{IR}}}{L_{\text{Edd}}}) \rangle$	$\langle \frac{f(25)}{f(60)} \rangle$
(1)	(2)	(3)	(4)	(5)
Type I ULIRGs	12.37 (0.30)	7.26 (0.84)	0.525 (0.74)	0.270 (9.8×10^{-2})
QSOs	11.56 (0.51)	8.33 (0.68)	–1.06 (0.55)	0.766 (0.33)

Note.-Col. (1): Name of subgroup. Col. (2): Average infrared luminosity and its dispersion, except for objects with upper and lower limits. Col. (3): Average black hole mass and its dispersion. Col. (4): Average $L_{\text{IR}}/L_{\text{Edd}}$ and its dispersion, except for the with upper and lower limits. Col. (5): Average $\frac{f(25)}{f(60)}$ and its dispersion, except for objects with upper and lower limits. Type I ULIRG = ultraluminous infrared galaxies with type I Seyfert nuclei.

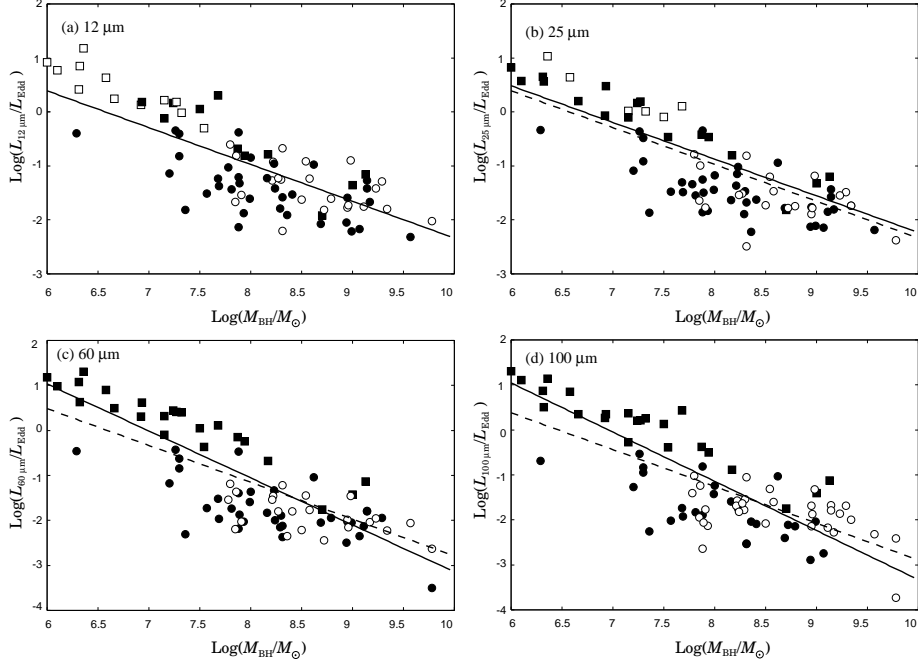


Fig. 1.— (a) Ratio of 12- μm luminosity, defined as νL_{ν} , to active galactic nuclei (AGN) Eddington luminosity ($L_{12\mu\text{m}}/L_{\text{Edd}}$) vs. black hole mass (M_{BH}) for 23 ultraluminous infrared galaxies with type I Seyfert nuclei (squares) and 58 PG QSOs (circles). Open symbols denote the upper limit. The best-fitting relationship (solid line) for all targets except for the upper limit data was $\log(L_{12\mu\text{m}}/L_{\text{Edd}}) = -0.687(\pm 0.135) \log M_{\text{BH}} + 4.98(\pm 1.0)$, with $\chi^2 = 0.248$. (b) Same as (a), but the abscissa are for the ratio of the 25- μm luminosity to AGN Eddington luminosity, $L_{25\mu\text{m}}/L_{\text{Edd}}$. The best-fitting relationship (solid line) for all targets except for the upper limit data was $\log(L_{25\mu\text{m}}/L_{\text{Edd}}) = -0.816(\pm 0.075) \log M_{\text{BH}} + 5.39(\pm 0.60)$, with $\chi^2 = 0.254$. For comparison, we overplotted the best-fitting relationship of $\log(L_{12\mu\text{m}}/L_{\text{Edd}})$ vs. $\log M_{\text{BH}}$. (c) Same as (a), but the abscissa are for the ratio of the 60- μm luminosity to AGN Eddington luminosity, $L_{60\mu\text{m}}/L_{\text{Edd}}$. The best-fitting relationship (solid line) for all targets except for the upper limit data was $\log(L_{60\mu\text{m}}/L_{\text{Edd}}) = -1.04(\pm 0.099) \log M_{\text{BH}} + 7.19(\pm 0.78)$, with $\chi^2 = 0.46$. (d) Same as (a), but the abscissa are for the ratio of the 100- μm luminosity to AGN Eddington luminosity, $L_{100\mu\text{m}}/L_{\text{Edd}}$. The best-fitting relationship (solid line) for all targets except for the upper limit data was $\log(L_{100\mu\text{m}}/L_{\text{Edd}}) = -1.09(\pm 0.115) \log M_{\text{BH}} + 7.50(\pm 0.89)$, with $\chi^2 = 0.49$.

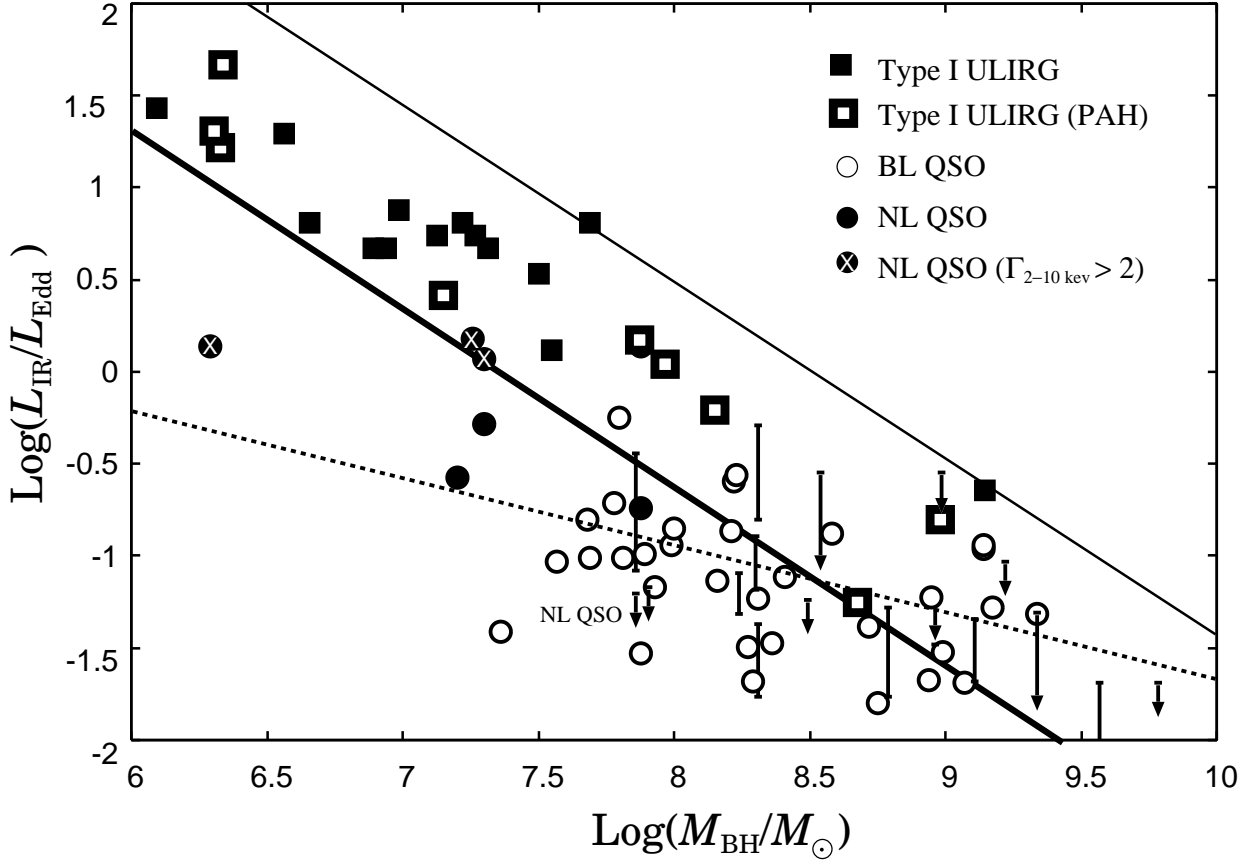


Fig. 2.— Ratio of infrared to Eddington luminosity ($L_{\text{IR}}/L_{\text{Edd}}$) vs. black hole mass for 23 ultraluminous infrared galaxies with type I Seyfert nuclei (type I ULIRGs; squares) and 58 PG QSOs (circles + down arrows). Open squares are type I ULIRGs in which polycyclic aromatic hydrocarbon emissions were detected. Filled circles show narrow-line QSOs (NLQSOs), and filled circles with crosses denote NLQSOs with $\Gamma_{2-10\text{keV}} > 2$. The thick solid line denotes the linear regression for all targets (type I ULIRGs and PG QSOs) except those with upper limit data. The best-fitting relationship for all targets was $\log(L_{\text{IR}}/L_{\text{Edd}}) = -0.961(\pm 0.081) \log M_{\text{BH}} + 7.06(\pm 0.65)$, with $\chi^2 = 0.319$. The dotted line represents the best fitting relation for broad-line QSOs only, except for the upper limit data, $\log(L_{\text{IR}}/L_{\text{Edd}}) = -0.369(\pm 0.11) \log M_{\text{BH}} + 1.89(\pm 0.028)$, with ($\chi^2 = 0.149$). The thick and thin solid lines correspond to $L_{\text{IR}} = 10^{12} L_{\odot}$ and $L_{\text{IR}} = 10^{13} L_{\odot}$, respectively (see §4.2 for details).

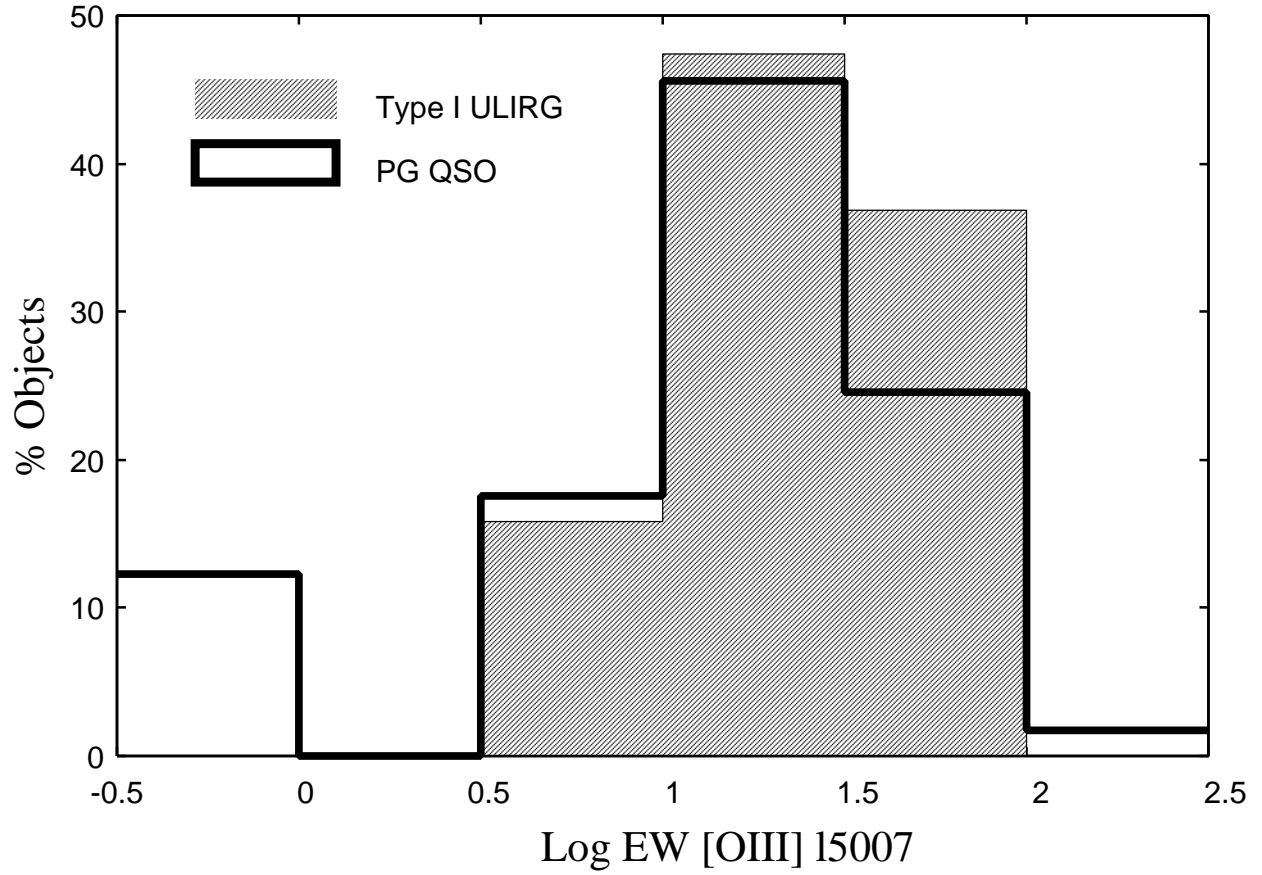


Fig. 3.— Equivalent width of [O III] λ 5007 (rest frame) histogram. *Shaded bars:* The distribution of EW[O III] λ 5007 (rest frame) for ultraluminous infrared galaxies with type I Seyfert nuclei (type I ULIRGs). *Open bars:* The distribution of EW[O III] λ 5007 (rest frame) for PG QSOs.

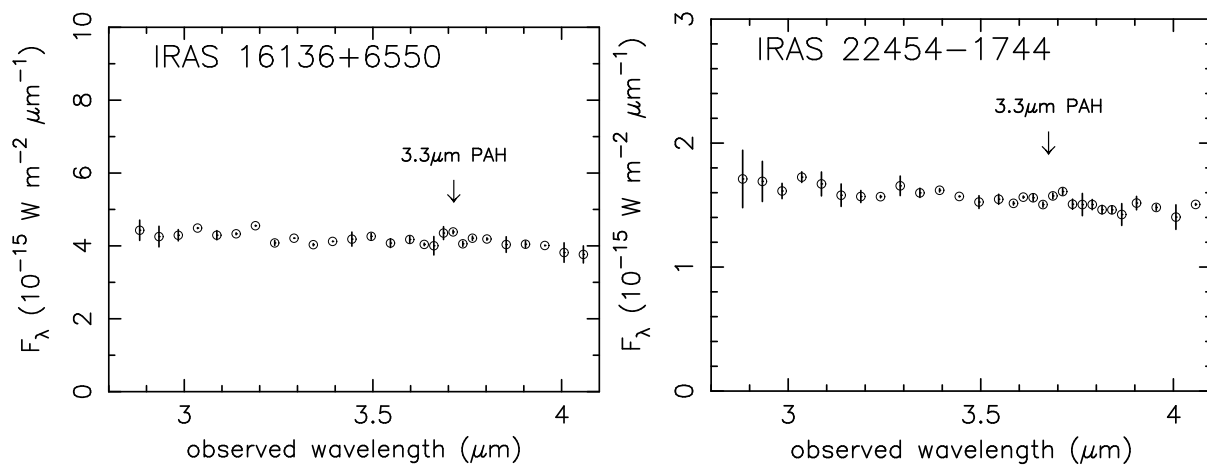


Fig. 4.— Infrared L -band ($\lambda_{\text{obs}} = 2.8\text{--}4.1 \mu\text{m}$) spectra of the two ultraluminous infrared galaxies with type I Seyfert nuclei (type I ULIRGs). The abscissa and ordinate are the observed wavelength in μm and F_{λ} in $10^{-15} \text{ W m}^{-2} \mu\text{m}^{-1}$, respectively. The down arrows with $3.3\text{-}\mu\text{m}$ PAH (polycyclic aromatic hydrocarbon) indicate the expected wavelength of the $3.3\text{-}\mu\text{m}$ PAH emission ($\lambda_{\text{rest}} = 3.29 \mu\text{m}$).